



## OPEN Systolic blood pressure estimation method using electrocardiogram RRI data

Etsunori Fujita<sup>1</sup>✉, Ryuichi Uchikawa<sup>1</sup>, Yumi Ogura<sup>1</sup>, Yoshika Nobuhiro<sup>1</sup>, Shinichiro Maeda<sup>1</sup>, Shigeyuki Kojima<sup>1</sup>, Koji Maeno<sup>2</sup>, Shigeyuki Igarashi<sup>2</sup>, Teruyo Kitahara<sup>3</sup>, Hiroji Tsujimura<sup>3</sup>, Kazushi Taoda<sup>4</sup>, Tomohiko Kisaka<sup>5</sup>, Kohji Murata<sup>6</sup> & Masao Yoshizumi<sup>7</sup>

Having obtained an idea from the Guyton model appertaining to the arterial pressure control mechanisms, we propose a novel chaos time series analysis method working with the non-nervous intermediate pressure control mechanism. Responses of the intermediate pressure control mechanisms are obtained from an electrocardiogram RRI delay coordinate system, and two frequency ranges are determined via residual functions to identify action and compensation by using the two best approximation functions. Absolute values of objects for control are estimated with the gradients of tangent and quantities of state at the inflection points of the best approximation functions. We obtained a polynomial determining a three-dimensional response surface ( $R^2 = 0.814$ ) that converted the two gradients of tangent calculated from the electrocardiogram RRI data of 225 cases and brachial systolic blood pressure into quantities of state. Further, the estimated values obtained by inputting the electrocardiogram RRI data of 120 readings from one subject into this polynomial showed strong correlation ( $R^2 = 0.8564$ ) with the measured brachial systolic blood pressure. Thus, it showed that the gradients of tangent were parameters grasping chaotic variation of the intermediate pressure control mechanisms.

**Keywords** Long-term blood pressure regulation mechanism, Short-term blood pressure regulation mechanism, Intermediate pressure control mechanism, Residual function, Best approximation curve, Three-dimensional response surface converting

### Abbreviations

CFSM	capillary fluid shift mechanism
ECG	electrocardiogram
e SBP	estimated systolic blood pressure
GT	gradient of tangent
GT of LTM	gradient of tangent of LTM
GT of STM	gradient of tangent of STM
IP	inflection point
IPCM	non-nervous intermediate pressure control mechanisms
IPn (n=1 to 3)	frequency at inflection point
ITn (n=1 to 3)	frequency at intersection of tangent
LSR	frequency range, lower than OLR, in which general physiological phenomena related to LTM acts
LTM	long-term mechanisms of IPCM (0.006~0.017Hz)
Mean	mean value
OLR	frequency range between upper side limit and lower side limit

<sup>1</sup>Delta Tooling Co., Ltd, 1-2-10 Yanoshinmachi Aki-ku, Hiroshima City, Hiroshima 736-0084, Japan. <sup>2</sup>Fukui-ken Saiseikai Hospital, Funabashi 7-1, Wadanaka-cho, Fukui City, Fukui 918-8503, Japan. <sup>3</sup>Division of Occupational and Environmental Health, Shiga University of Medical Science, Seta Tsukinowa-cho, Otsu City, Shiga 520-2192, Japan. <sup>4</sup>Biwako Professional University of Rehabilitation, 967 Kitasaka-cho, Higashiomi City, Shiga 527-0145, Japan. <sup>5</sup>Hakuaikai Kisaka Hospital, 1235 Saijocho Doyomaru, Higashihiroshima City, Hiroshima 739-0003, Japan. <sup>6</sup>Graduate School of Nursing, Sanyo Gakuen University, 1-14-1 Hirai, Naka-ku, Okayama City, Okayama 703-8501, Japan. <sup>7</sup>Yasuda Women's University, 6-13-1 Yasuhigashi, Asaminami-ku, Hiroshima City, Hiroshima 731-0153, Japan. ✉email: gonzo@deltatooling.co.jp

PAC	premature atrial contraction
PVC	premature ventricular contraction
RAS	renin-angiotensin system
RAVS	renin-angiotensin vasoconstriction system
RRI	R-R interval
SBP	systolic blood pressure
SD	standard deviation
SRMV	stress-relaxation mechanism of the vasculature
STM	short-term mechanisms of IPCM (0.017~0.06Hz)
USR	frequency range, higher than OLR, having the maximum trajectory frequency in which STM acts

Arterial pressure is not regulated by a single pressure control system, but instead by several interrelated, integrated and multifaceted systems. It is controlled via short-term blood pressure control (p215-225)<sup>1</sup> starting with nervous control mechanisms before shifting to non-neural intermediate pressure control mechanism (hereafter abbreviated as IPCM, p241-243)<sup>1</sup> and stabilized via the long-term blood pressure control mechanisms (p227-243)<sup>1</sup>. This mechanism of long-term stabilization includes multiple interactions with the renin-angiotensin system (hereafter abbreviated as RAS), the nervous system, and various other regulatory factors (p215-225, P227-243)<sup>1</sup>.

The Guyton model advocates (1) renin-angiotensin vasoconstriction system (hereafter abbreviated as RAVS) functioning by a unit of minutes or hours, (2) stress-relaxation mechanism of the vasculature (hereafter abbreviated as SRMV), and (3) IPCM of CFMS. (1) RAVS is clear as a frequency, but for (2) SRMV and (3) capillary fluid shift mechanism (hereafter abbreviated as CFMS), frequencies are not reflected, and the examination on transient response regarding IPCM has not been deliberated enough. Accordingly, in the present study, we examined the transient response of IPCM focusing on a vibration model.

The pressure control of RAS is performed in the frequency range between 0.006 and 0.017 Hz (p235)<sup>1</sup>, while the nervous arterial pressure control is conducted between 0.017 and 0.1 Hz (p218)<sup>1</sup>. The difference between these regulatory frequencies produces a phase difference, which results in determining a working frequency range of IPCM. Here, IPCM that works in the frequency range between 0.006 and 0.017 Hz is called Long-Term Mechanisms of IPCM (hereafter abbreviated as LTM), while the IPCM that works in the frequency range between 0.017 and 0.06 Hz, considering the buffer action (0.0476Hz<sup>2</sup>) (p221)<sup>1</sup> of the baroreceptor, is called Short-Term Mechanisms of IPCM (0.017 ~ 0.06 Hz) (hereafter abbreviated as STM). Thus, IPCM is examined by dividing it into the two frequency ranges. Since the regulation via IPCM is performed within the wide frequency range from 0.006 to 0.06 Hz, a double logarithmic axes display is useful for analysis related to arterial pressure regulation.

The Guyton theory (p225)<sup>1</sup> explains the characteristics of arterial pressure control by the nervous system from an engineering perspective. It says that “any reflex pressure control mechanism can oscillate if the intensity of ‘feedback’ is strong enough and if there is a delay between excitation of the pressure receptor and the subsequent pressure response. The vasomotor waves illustrate that the nervous reflexes that control arterial pressure obey the same principles as those applicable to mechanical and electrical control systems. If the feedback ‘gain’ is too great, and there is also delay in response time of the arterial pressure control mechanisms, oscillation with large amplitude occurs at a lower frequency than that in a normal state.”

A response having a large gain and producing a short reaction time delay is an impulse response. The combination of reciprocal step responses becomes an impulse response. These reciprocal responses in a vibration model system approximate the relationship between action force and compensation force in a biological system.

The biological system makes reciprocal properties coexist within a certain range of frequencies. As a result, there occurs fluctuation<sup>3</sup>, which has a similar role to a damping ratio. Fluctuation exists between the action and compensation of the responses of the arterial pressure control by LTM and STM, and a phase difference occurs in the step responses due to the buffer action<sup>4</sup> of the fluctuation. Accordingly, we believed that the fluctuation in a certain range of frequencies within a frequency response curve would correspond to the damping ratio calculated on a Bode diagram.

## Methods

Here, the Guyton extended model, the data processing method, and the devised analysis method will be explained.

For the data processing flow, we first conduct an Abnormal Value test.

We extract the R-R interval (hereafter abbreviated as RRI) of an electrocardiogram (hereafter abbreviated as ECG) to create a Lorenz plot and Attractor, to calculate mean value (hereafter abbreviated as Mean) and standard deviation (hereafter abbreviated as SD) from the RRI Attractor, and to create a Mean-SD correlation diagram.

Using these diagrams, we extract outliers, which are to be rejected from the ECG RRI time series data.

Successively, from ECG RRI time series data, we conduct  $\theta_{i-0}$  time series analysis (Ensemble average), and create a  $\theta_{i-0}$  spectrum diagram from the  $\theta_{i-0}$  time series analysis data.

We compare the  $\theta_{i-0}$  spectrum diagram with the instantaneous heart rate spectrum diagram. We check that the energy variation indexes are expressed with frequency gradients, from the motion modes of fluctuation of the control mechanisms in the frequency ranges. We then create an IPCM approximation curve relative to a power spectrum between 0.006 and 0.06 Hz. We calculate the residual between the IPCM approximation curve and the power spectrum to create an IPCM residual function. Setting the IPCM residual function as the border, we create two residual probability distribution curves (high group and low group). Using the residual probability distribution curve, we limit frequency ranges for analysis, and create residual functions related to

LTM and STM. From the method of separating power spectra of LTM and STM using the residual functions, we determine the frequency ranges for analysis. Using the power spectra within the determined frequency ranges, best approximation curves are created, and we calculate the frequency gradients related to LTM and STM.

Using the two calculated frequency gradients and measured blood pressure values, we create a three-dimensional response surface, and using a quartic polynomial expressing the characteristics of the response surface, we can estimate SBP (hereafter abbreviated as e SBP).

### Experimental method

In accordance with the Declaration of Helsinki, this study was approved by the ethics committees within the Delta Tooling Co. Ltd, Shiga University of Medical Science and Fukui-ken Saiseikai Hospital, and informed consent was obtained from the subjects by explaining the purpose and contents of the experiment to be conducted.

The subjects of the experiment were people aged from their 20 s to their 90 s with natural respiration in a resting and sitting position. The experiment (test) was conducted only once per subject using an electrocardiograph in a group of subjects who were healthy and not outpatients (88 subjects), and a group of outpatients having cardiovascular diseases such as cardiac diseases, hypertension, gout, diabetes, dyslipidemia, et cetera, and risk factors associated with these diseases (49 subjects), giving a total of 137 subjects. In Supplementary Table S1, the subjects' background information of this study is shown. In Delta Tooling Co. Ltd, Shiga University of Medical Science, and Fukui-ken Saiseikai Hospital, for brachial systolic blood pressure, the mean of the two measured values was recorded. SBP of the 137 subjects (225 cases) in a resting and sitting state was measured for 45 s with a brachial sphygmomanometer, the heart rate data for 360 s was collected by using an electrocardiograph, wearing the sphygmomanometer, and SBP after the experiment was measured with the brachial sphygmomanometer. In Supplementary Fig. S4, the protocol of measurement with an electrocardiogram and blood pressure measurement is shown. To take the uncertainty into consideration, the mean value of the brachial systolic blood pressures before and after the measurement time of the heart rate data for 360 s was taken, and in cases where there was a difference of more than 5 mmHg between the two measured values, three or four measurements were conducted, and the mean of the two measured values closest to each other was recorded. The measurement places were set up in the three places mentioned in the opening paragraph of this section. In Delta Tooling Co. Ltd and Shiga University of Medical Science, the experiments were performed by installing vehicle seats in experimental jigs, while in Fukui-ken Saiseikai Hospital, relaxing chairs were used. The experimental equipment, those carrying out experiments, the subjects, the person in charge of analysis, and the seasons in which the experiments were performed all differ.

In all three locations, the mean of two measured values of brachial SBP was recorded. However, in cases where there was a difference of more than 5 mmHg between the two measured values, three or four measurements were conducted, and the mean of the two measured values closest to each other was recorded. In Delta Tooling Co. Ltd, multiple measurement experiments of the same subjects were conducted. In the multiple measurements, in cases where data of the measured blood pressure variation range exceeded 20 mmHg, they were analyzed by specifying the minimum, average and maximum values.

Further, a blood pressure measurement experiment was also performed with the cooperation of a 67-year old subject for one year, maintaining normotension to elevated blood pressure by medication (120 measurements) over this period.

## Results

### Abnormal value test

On the basis of the Guyton extended model, data processing method and devised analysis method, the results of the analysis and experiments will be explained below.

In the Fig. 1 flowchart, relative to the ECG RRI data having irregular rhythms, attractors of a dynamical system were created applying chaos time series analysis, and from their behavior, they were classified into Quasi-periodicity (A) and Chaos (B).

The irregular rhythms are due to the dynamics of a non-linear mechanical system with a few degrees of freedom<sup>5</sup>. When using the correlation diagram of Mean-SD regarding the attractors, even allowing for said freedom, stochastic phenomena can be extracted. A line drawn at 45° creates a border line where 70% of the data exists within the range of Mean, and was set as the criteria on the correlation diagram of Mean-SD. The attractors were divided into two regions: the one representing quasi-periodicity behavior on one side of the line, and the one indicating chaotic behavior on the other.

Figure 1 (1) shows the ECG RRI data, (2) shows the instantaneous heart rate time series data calculated from the RRI data, and (3) shows the attractors reconstructed in a three-dimensional delay coordinate system. The attractor of (A) became a torus attractor (○), and the reference plane of the three-dimensional delay coordinate system was filled with two-dimensional tori. In (B), in addition to the torus attractor, an attractor having a fractal structure was generated, which became a strange attractor. The points of the instantaneous heart rate constituting the attractors were plane-approximated via the least squares method to obtain the reference plane of the attractors, and the Mean and SD of the distances of the points of the Attractors from the reference plane were calculated to plot them in the correlation diagram of Mean-SD<sup>6</sup> of (4). The regression expression of the cluster of (A) was expressed with a quartic function, but its quartic to quadratic coefficients were small, becoming closer to a linear function. The regression expression of the cluster of (B) was expressed with a quadratic function, which showed non-linear behavior. When the Mean became larger, it would sometimes cross the 45° line. This suggests that when the proportion of the attractors showing chaotic behavior increased, it may change to have quasi-periodicity behavior<sup>7</sup>.

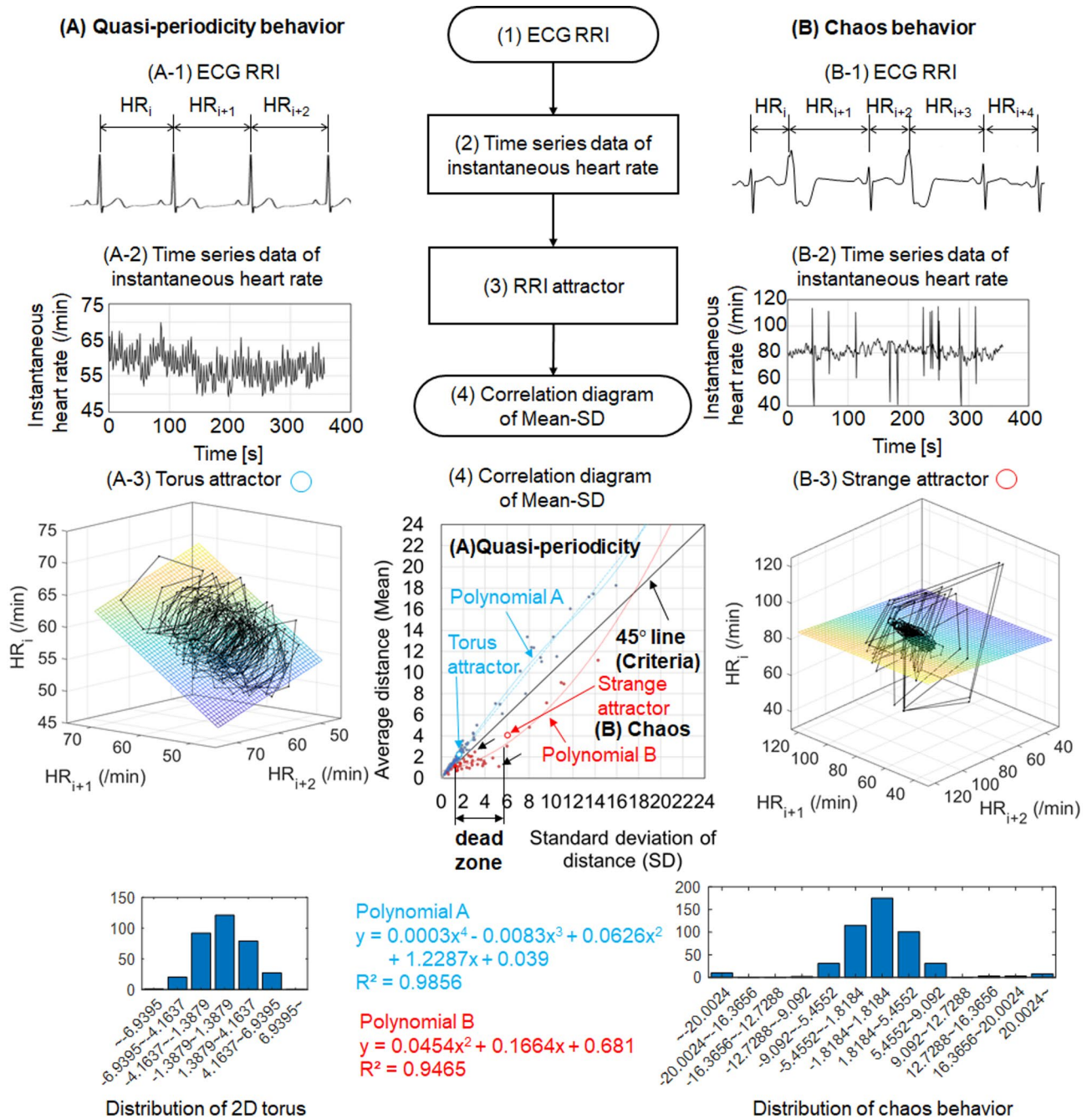


**Fig. 1.** Flowchart of correlation diagram of Mean-SD. ECG RRI was converted from an observation time series into a time delay coordinate system. From the ECG RRI (1), the instantaneous heart rate (2) was calculated, and the attractor trajectory (RRI attractor) in a three-dimensional delay coordinate system and its residual density function (histogram) were created (3). (A-3) was a torus attractor (○), and (B-3) became a strange attractor (○). The histogram of the torus attractor became a normal distribution. The histogram of the strange attractor became a superposition of negative kurtosis and normal distribution. (A) and (B) were low-dimensional chaos, with (A) showing quasiperiodic behavior, and (B) showing chaotic behavior. With the analysis results of the 225 cases of the 137 subjects, the correlation diagram of Mean-SD (4) was created. Setting a 45° line on the correlation diagram of Mean-SD as the criteria, it was divided into two clusters of (A) and (B). The Polynomial A of the correlation diagram of Mean-SD was expressed with a quartic function closer to a linear function, while the Polynomial B was a Duffing’s equation and expressed with a quadratic function having a non-linear dead zone and a range closer to a linear function. The existence of outliers or abnormal values is suggested in the instantaneous heart rate time series data, with attractor trajectories having a Mean-SD relationship existing in the range of the dead zone. The procedures for the detection of outliers by using the instantaneous heart rate time series data and of the abnormal value test using ECG, Lorenz plot and RRI attractors are explained in Fig. 2

The coefficient of the linear term of the quartic function existing in the region showing quasi-periodicity behavior is 1.2287 and shows linear behavior. Its dispersion is closer to a normal distribution, which makes noise intervention unlikely.

For the quadratic and linear terms of the quadratic function existing in the region representing chaotic behavior, their SD became coefficients indicating a dead zone in the range between 1 and less than 6. In particular, the range between the line at 45° and the quadratic function indicated by an arrow, and the range where the Mean has little variation relative to SD are dead zones. In the dead zones, even if the variation of Mean is little, the variation of SD becomes large and an unstable state. If Mean and SD are small, the variations are small and the stability increases. When Mean and SD become large, they deviate from the dead zones. The gradient of the quadratic function became closer to the gradient of the region indicating quasi-periodic behavior, showing linear behavior.

Accordingly, dead zones were set as the ranges that met the following three conditions, which were ranges that needed noise rejection:

- (1) SD exists in the ranges of 1 to 6.
- (2) SD is between the regression expression of (B) and the line at 45°.
- (3) The coefficient of the linear term is not corrected with the quadratic term.

The strange attractor (○) showing chaotic behavior in Fig. 1 (B) is in the dead zone, and is the subject of an abnormal value test. The chaotic behavior was due to the formation of premature ventricular contraction (hereafter abbreviated as PVC), and was repeated on the instantaneous heart rate time series data. Since it repeated, the attractor trajectory could be divided into PVC and other states. Analysis conducted regarding this case is shown in Supplementary Fig. S2. In the case of PVC repeating, there occurs a phenomenon called 'dispersion and concentration' in the relation between the best approximation curve and the power spectra. This 'dispersion and concentration' is reflected on the gradient of tangent (hereafter abbreviated as GT). For instance, the best approximation curve shown in Fig. 6 (3) and the best approximation curve shown in Supplementary Fig. S2 (8) correspond, but their GTs are different. This difference in the result of calculating GTs occurred due to a difference between using a tangent line of an inflection point (hereafter abbreviated as IP) or a double tangent to be determined as a GT, in accordance with the 'dispersion and concentration' of the power spectra within a frequency range having the maximum trajectory frequency in which STM acts, higher than the frequency range between the upper side limit and lower side limit; upper side frequency range is hereafter abbreviated as USR, while overlap range is hereafter abbreviated as OLR.

Figure 2 is a flowchart of an abnormal value test. The two cases (A) and (B) existing in the dead zone of the correlation diagram of Mean-SD shown in Fig. 2 (C) were carefully examined.

The case shown in Fig. 2 (A) represents quasi-periodicity behavior, in which heart rate was both fast and slow over an extended length of time as shown in (A-1) and (A-3). Outliers were rejected from the instantaneous heart rate time series data shown in (A-2), and the data was replotted on the correlation diagram of Mean-SD shown in Fig. 2 (C). As the variation was small before and after the rejection of the time series data, (A) was judged as a case in which the data could be retained.

The case shown in Fig. 2 (B) represents chaotic behavior, in which premature atrial contraction (hereafter abbreviated as PAC) occurred. Outliers were rejected from the instantaneous heart rate time series data, and the data was replotted on the correlation diagram of Mean-SD shown in Fig. 2 (C). As the variation was large before and after the rejection of the time series data, (B) was deemed to be a case in which the data should be rejected.

The irregular behavior existing in the instantaneous heart rate time series data of the subjects was examined using two analysis methods: ECG time series waveforms, and chaos time series data analysis. In cases where the dispersion factors reside in the system, errors take on a normal distribution. This state in (A) is quasi-periodicity behavior.

In contrast, (B) shows chaos behavior, and is a case where the dispersion factors are due to modification via other systems. (B) had repeated PVC shown in Fig. 1 (B) and a single PAC shown in Fig. 2 (B). The PVC case became time series data in which two heart rate variabilities were superimposed grasping a standard RRI at rest and an RRI with wide QRS via ectopic ventricular excitation. In the PVC case, from the ensemble average of the reconstructed two-dimensional delay coordinate system, two clusters occurred: one having an oval shape at Mean, and a second dispersing in the periphery. Since the two clusters were dispersion caused by cardiac contraction and influence of nervous control, the best approximation curves became similar through repetition. The appearance of the two clusters was reflected on the frequencies and the power spectra, which resulted in producing the difference of the GTs.

In the case of a single PAC shown in (B-1) and (B-2) in Fig. 2 (B), the axis angle of the short-term ensemble average deviates by a large amount as shown in (B-3), and an outlier is generated in the  $\theta_{i-0}$  time series data. The frequency of the outlier becomes  $1/30 \text{ sec}^{-1} = 0.033 \text{ Hz}$ , and the outlier is reflected on the power spectrum in the range between 0.006 and 0.06 Hz, affecting GT. Accordingly, the number of noises related to the frequency also becomes a constraint condition. For the case of a single PAC, as shown in (B-4) and (B-5) the factors given to the best approximation curves could be removed by discarding the PAC portion.

### $\theta_{i-0}$ time series analysis (ensemble average)

The instantaneous heart rate time series data is reconstructed in two-dimensional state space via a Lorenz plot. From the angle variation of the ensemble average for 30 s relative to the principal axis angle  $\theta_0$  of the ensemble average for 360 s,  $\theta_{i-0}$  time series data is created, and a spectral diagram is produced via frequency analysis. A flowchart for creating a spectral diagram and analysis examples is shown in Fig. 3. The angle information on these ensemble averages is time series data in which phenomena such as trajectory instability due to non-linear

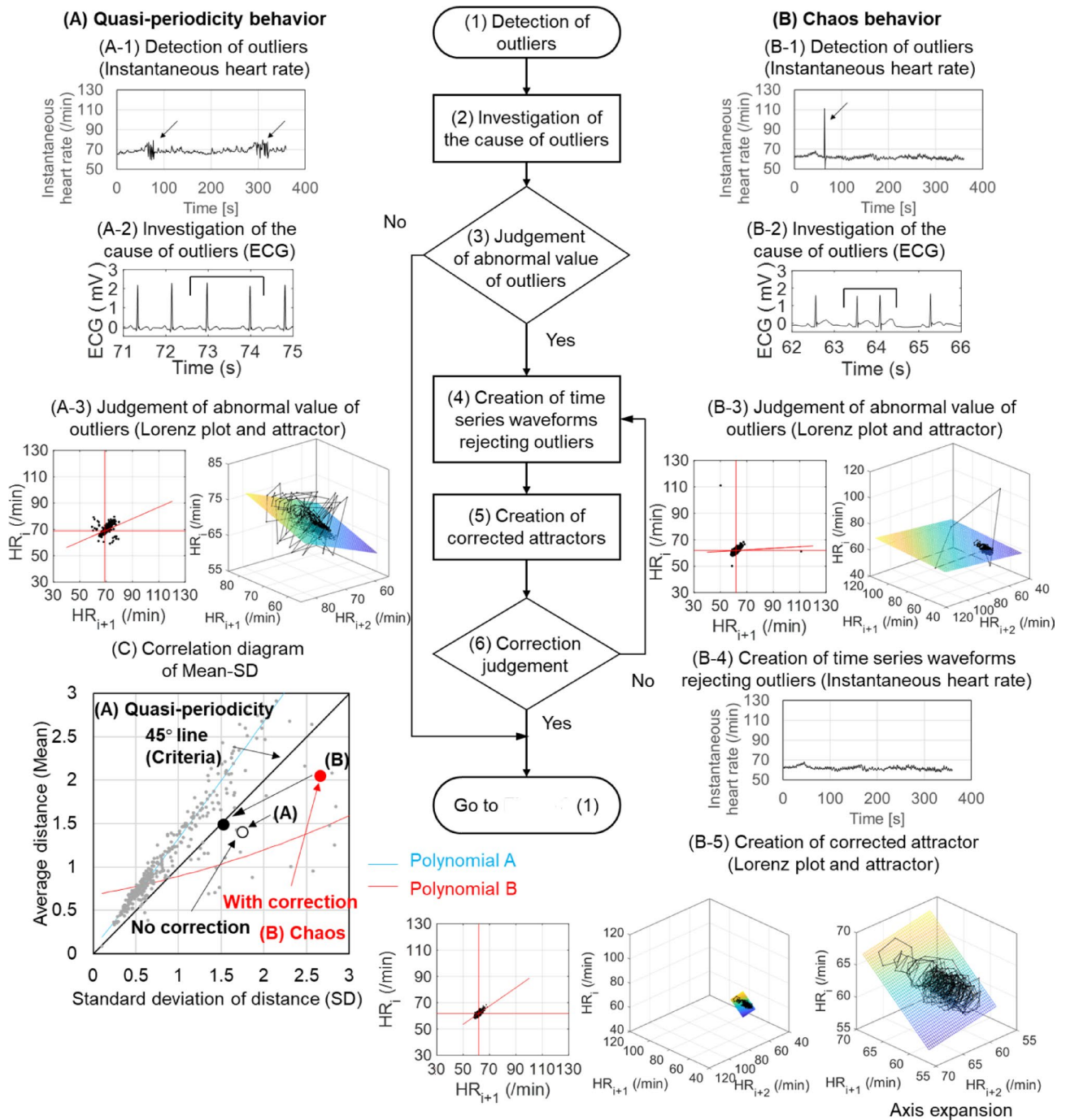


**Fig. 2.** Flowchart of abnormal value test. Cases having an irregular rhythm range in the instantaneous heart rate data (the arrow part of A-1, Quasi-periodicity behavior (A)) and having one outlier (the arrow part of B-1, Chaos behavior (B)) were extracted from the 225 cases. The irregular rhythm range was judged as normal sinus rhythm, since it was caused only by an extension of RRI in ECG (A-2). The outlier was judged that it was caused by the formation of PAC in ECG (B-2). For the RRI Attractor, the former was not an abnormal value (A-3), while the latter could be judged as an abnormal value (B-3). From both RRI Attractors, Mean and SD were calculated, and when plotting them on the correlation diagram, they were in the dead zone (C). Accordingly, the waveform due to PAC was excluded from the instantaneous time series data of (B-1), and a correction was made (B-4). Successively, the corrected Lorenz plot and the corrected attractor were created (B-5). From the corrected RRI Attractor, Mean and SD were calculated, and when they were replotted on the correlation diagram of Mean-SD, they moved to the vicinity of the 45° line (●)(C). The ensemble average in the Lorenz plot diagram shown in (A-3) becomes a method of reducing the effects of outliers. A data processing method of converting angle information of the ensemble average into a parameter was devised. This procedure is shown in Fig. 3

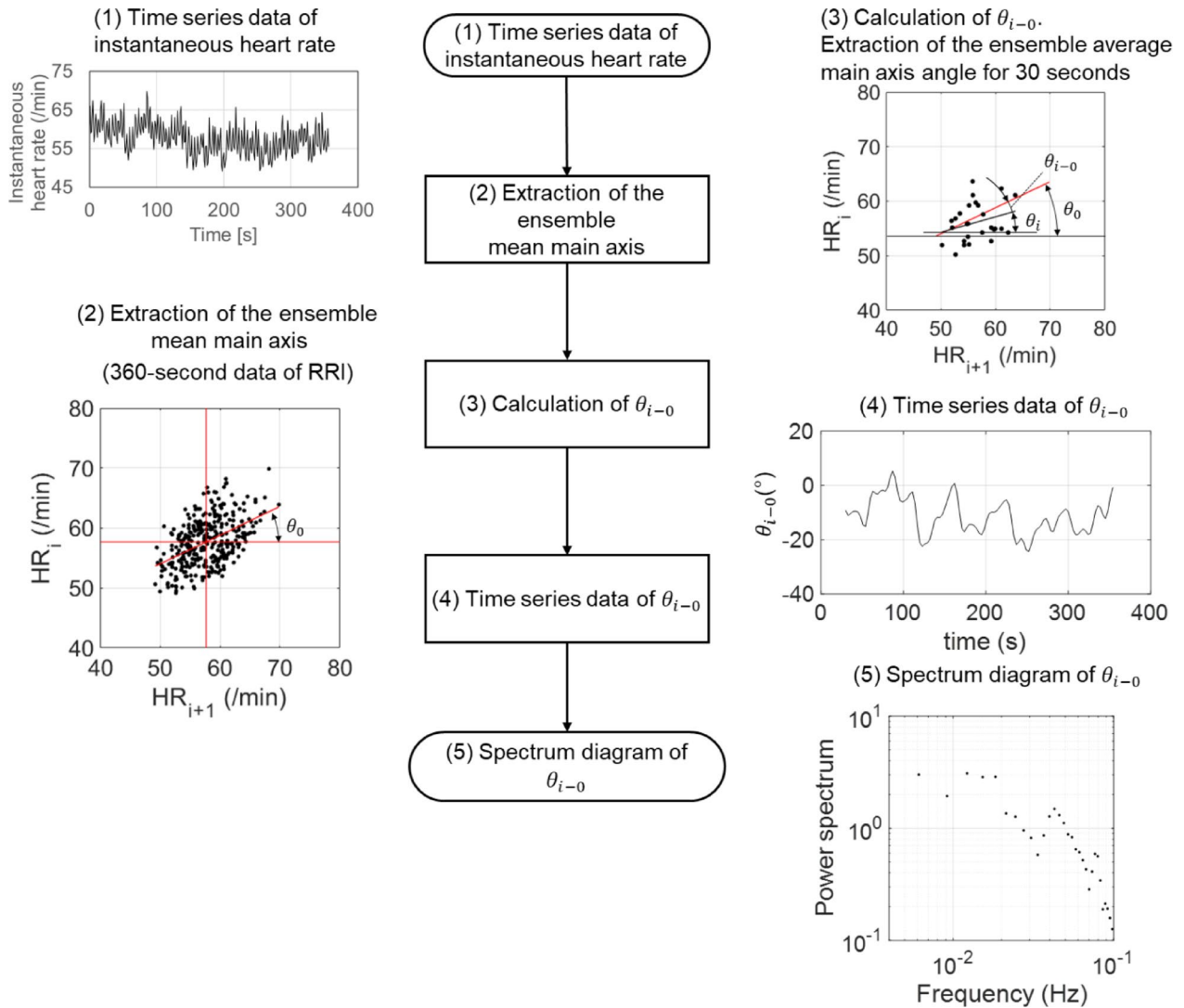
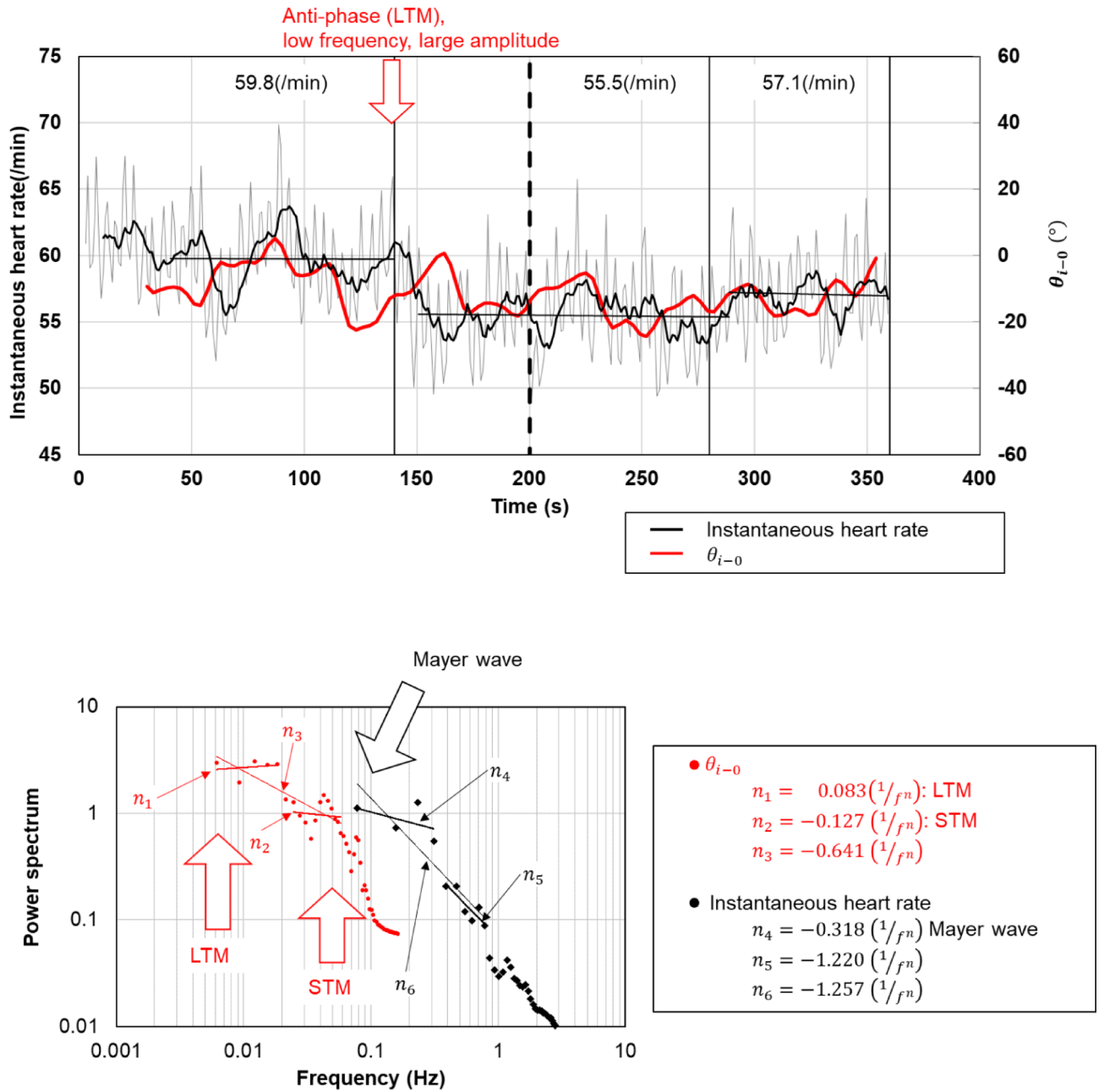


**Fig. 3.** Flowchart: spectrum diagram of  $\theta_{i-0}$ . The instantaneous heart rate time series data was created (1) and the angle  $\theta_0$  of the main axis was set from the ensemble average (for 360 s) of the two-dimensional delay coordinate system (2). The angle  $\theta_i$  of the main axis of the ensemble average for 30 s was calculated to establish the angle difference  $\theta_{i-0}$  from the main axis set with the data for 360 s (3). The  $\theta_{i-0}$  time series data regarding the angle information was created (4), which was frequency-analyzed to obtain the spectrum diagram (5). On the basis of the energy variation information originated in the power spectra obtained through these analysis methods, a method of quantification is examined, which quantitatively expresses the robustness and plasticity of the control mechanism shown in Fig. 4.

dynamical system, fractality of Attractor and non-periodicity reside. By performing frequency analysis of this time series data, energy information could be obtained. By limiting frequency ranges to create an approximation function as an ideal curve, it was possible to estimate a regulation region, and by calculating residuals, the dispersion degree of the active region could be identified.

Next, using the flowchart and analysis diagram of Fig. 3, the procedure for creating the ensemble average for decreasing the influence of irregular rhythms of a non-linear mechanical system with a few degrees of freedom will be explained. The instantaneous heart rate time series data with one variable (1) is reconstructed in a two-dimensional state space via a Lorenz plot, and the main axis angle  $\theta_0$  is calculated from the ensemble average for 360 s (2). Successively, the time series model:  $\theta_{i-0}$  time series data (4) is created, with the angle variation (3) calculated from the ensemble average for 30 s as a parameter, allowing frequency analysis to be conducted (5).

In Fig. 4, the times series analysis (1) combining the instantaneous heart rate time series data and  $\theta_{i-0}$  time series data, and the mechanism of GTs shown by the frequency analysis results (2) of this data is explained. Here, two frequency ranges were set in the parts of the power spectra that changed suddenly in the spectrum diagram when conducting frequency analysis of the instantaneous heart rate time series data and  $\theta_{i-0}$  time series data to calculate their GTs by using the least squares method.



(2) Frequency analysis result

**Fig. 4.** Instantaneous heart rate time series analysis/phase variation analysis ( $\theta_{i-0}$  time series analysis), and their frequency analysis. The heart rate variability time series waveforms that appeared as if they were locked on the three average heart rates were superimposed on the  $\theta_{i-0}$  time series waveforms reflecting phase information. With the instantaneous heart rate time series waveforms being periodical information and  $\theta_{i-0}$  time series waveforms being phase information, both waveforms became opposite movements between 100 and 200 s and resulted in anti-phase. There occurred phase deviation between both time series waveforms due to the reciprocal relationship between the action and compensation, and, as a result, a decrease in heart rate was recognized after 200 s onwards. Successively, a trade-off relation relative to this decrease worked between 250 s and 300 s, with the heart rate having a tendency to increase and become stable.

For time series analysis, a time series analysis diagram (1) having two axes, with instantaneous heart rate (/min) on the left coordinate axis and  $\theta_{i-0}$  (°) on the right coordinate axis. Heart rate fluctuated from 59.8/min to 55.5/min, and then to 57.1/min. At 200 s from the start of the measurement, there occurred anti phase of a low frequency with large amplitude at the timing when the heart rate decreased from 59.8/min to 55.5/min.

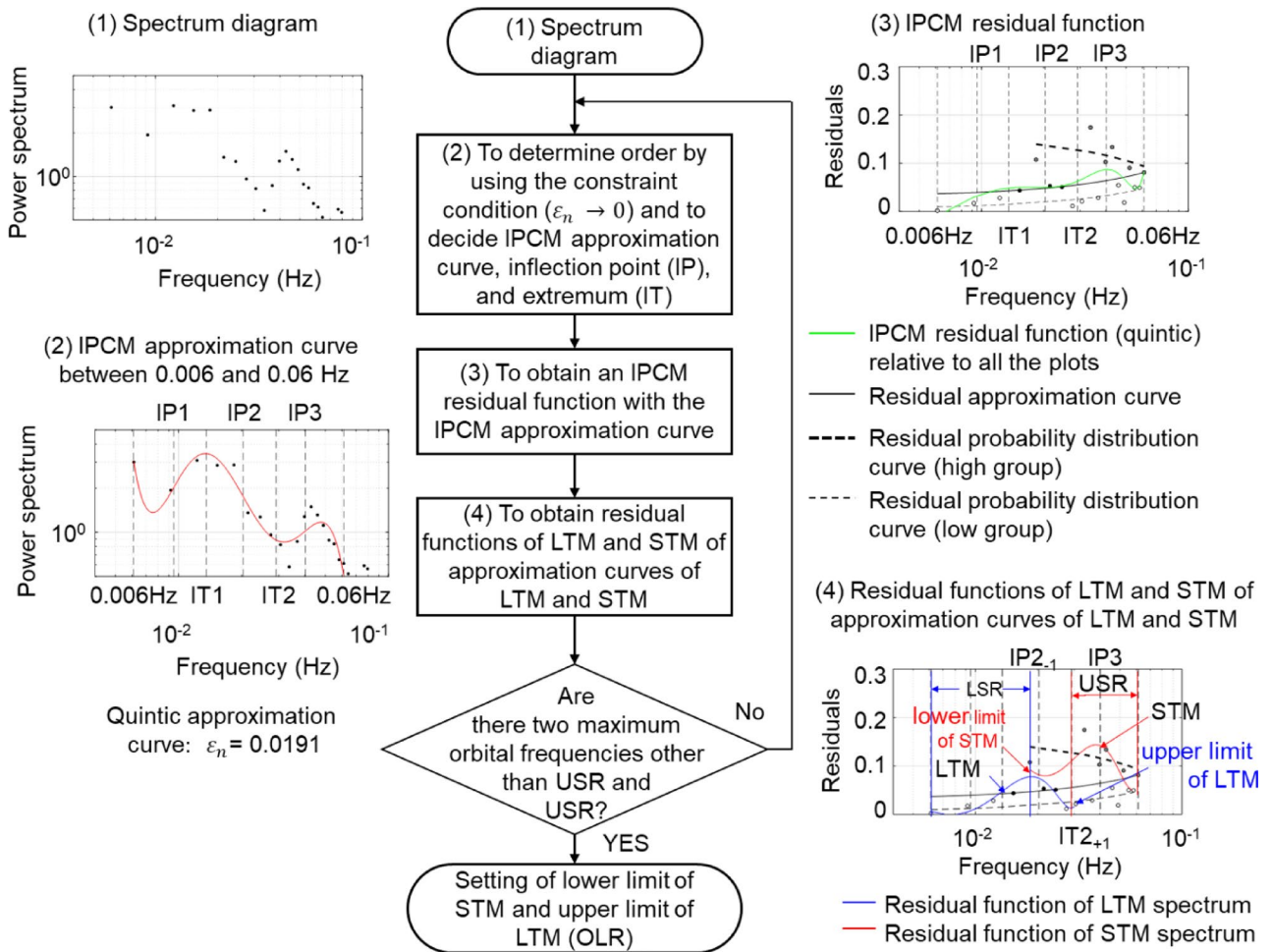


**Fig. 5.** Flowchart for determining the frequency ranges of LSR and USB. By using the  $\theta_{i-0}$  spectrum (1), the IPCM approximation curve (2) was expressed with a quintic function in the frequency range between 0.006 and 0.06 Hz. From the quintic function, IPs (IP1 to IP3) and intersections of tangent lines of IPs (IT1, IT2) were described (2). The vicinity of IP1, IT1 and IT2 having small residuals were active parts where the robustness of phase was high, while the vicinity of IP2 and IP3 having large residuals were defined as regulation sites where the plasticity of phase was high. The interval between IT2 having a small residual and IP2 having a large residual is free site<sup>8</sup> linking the two sites. Accordingly, by using the residuals between the approximation curve of the quintic function and spectra, an IPCM residual function diagram of a quintic function with residuals as the vertical axis and frequencies as the horizontal axis was created (3). For the residual function composed of the frequency range between 0.006 and 0.06 Hz, there occurred a stationary point in the vicinity of IP2 and the local maximum value in the vicinity of IP3. As a result, IP2 and IP3 become the maximum trajectory frequencies. Successively, using the least squares method, residual regression curves (residual approximation curves) were created to classify the residuals into two clusters. A regression curve created with the cluster having larger residuals than the regression curve was defined as the high group of the residual probability distribution curve, while a regression curve created with the cluster having smaller residuals was defined as the low group (3). Incidentally, the residual regression curves were created by making regression lines with the linear axis and expressing the frequencies on the horizontal axis with the logarithmic axis. The vicinity of the stationary point of the IPCM residual function became the maximum trajectory frequency of LTM, and the vicinity of the local maximum value became the maximum trajectory frequency of STM (4)

Macroscopically, when the amplitudes of both time series data became small, the heart rate decreased to become a stable fluctuation variation. It suggests that in the time zone until 200 s, when the two waveforms showed anti phase, the two control mechanisms became opposite movements (action and compensation), and from 200 s on, the decrease in heart rate and its stabilization occurred due to the nervous control. The instantaneous heart rate time series data and  $\theta_{i-0}$  time series data showed transient and stationary responses. Transient response characteristics to this kind of step response are decided by using three constants: their overshoot, rise time and setting time in Newtonian mechanics. The overshoot is a function having only a damping ratio, while the rise time and setting time are functions of natural frequencies and damping ratios. The natural frequencies are expressed with frequency information, while damping ratios are expressed with frequency information

and damping characteristics. The results of the frequency analysis of the  $\theta_{i-0}$  time series waveforms being phase information, become indexes of an energy function, and have information on the natural frequencies and damping ratios. Macroscopically, setting two frequency ranges of the  $\theta_{i-0}$  time series waveforms in the rapidly changing parts of the power spectra, and the GTs calculated with the least squares method were used as an index showing the plasticity of phase.

The GT of LTM becomes  $n_1 = 0.083$  and that of STM becomes  $n_2 = -0.127$ . GT of the fluctuation that maintains robustness and plasticity of blood pressure is  $n_3 = -0.641$ . GT of a Mayer wave is  $n_4 = -0.318$ . GT reflecting the excitation of the baroreceptor and the following delay between pressure reactions is  $n_5 = -1.220$ . The fluctuation that integrates these becomes  $n_6 = -1.257$ . The GTs of  $n_1 = 0.083$ ,  $n_2 = -0.127$  and  $n_4 = -0.318$  are the energy variation indexes of the control mechanism working to regulate each function of the organs in limited time zones.  $n_5 = -1.220$  and  $n_6 = -1.257$  showing  $1/f$  fluctuation are GTs that regulate the relationship between all of the organs in the body.

GTs obtained from the frequency analysis indicated the energy variation indexes of the low frequency component and the high frequency component relating to each response. For the control mechanisms in a human body, it was suggested that the moving mode of the control mechanisms was determined via the combination of fluctuations<sup>5,8,9</sup> in the range of frequency in charge of the control systems.

This timing of the change of time series waveform and change of state resembled the prediction of sleep phenomenon<sup>10</sup> in the previous study. Further, when the fluctuation became  $1/f$ , the residual between the regression equation and spectrum became small, but whenever the fluctuation was in the vicinity of 0 to 1, or when it had a gradient of +, the residual became large<sup>3</sup>. Accordingly, we believed that when action and compensation appeared, the residuals became large, while when control functions stabilized, the residuals became small, and the frequency ranges where the control mechanisms operated could be identified with the dispersion degree of the residuals.

### Method of separating power spectra of LTM and STM

By using the frequency range OSR between the upper side limit and lower side limit, a frequency range in which general physiological phenomena related to LTM act and is lower than OLR, is defined as LSR. In contrast, a frequency range having the maximum trajectory frequency in which STM acts and is higher than OLR, is defined as USR.

Figure 5 shows a method of determining the two frequency ranges (LSR, USR) of the  $\theta_{i-0}$  time series waveforms by using the residual functions.

From the spectrum diagram (1), an IPCM approximation curve was created using a quartic or quintic function (2). The order of the selected function was determined with the fitting parameter ( $\epsilon_n \rightarrow 0$ ). Successively, from the approximation curve, the frequencies of the IPs (hereafter abbreviated as IPn ( $n = 1$  to 3)) and those of the intersections of the tangent lines (hereafter abbreviated as ITn ( $n = 1$  to 3)) at the IPs were obtained (2). The inflection points and the intersection points of the two TLs on the IPCM approximation curve approximate the frequency of the geometric extrema, and the residuals tend to decrease, since the sign of the derivative function of the approximation curve switches at the extrema (2).

The residual between the IPCM approximation curve and spectra was calculated, and a correlation diagram between the residuals and frequencies duly generated. Using a quartic or quintic function, an IPCM residual function was created (3). The local minimum value of the residual function takes the minimum value of the residual. These two frequencies are called the minimum trajectory frequencies (3).

Successively, using the least squares method, a residual approximation curve indicating the Mean of the spectra was obtained. A residual probability distribution curve (high group) from the spectrum group having larger residuals than those of the residual approximation curve was created, along with a low group version for the spectrum group having smaller residuals than those of the residual approximation curve. With IPn ( $n = 1$  to 3), ITn ( $n = 1$  to 3) and the intersection between the two residual probability distribution curves (high group low group), residual functions related to LTM and STM were created (4). From the two residual functions, the lower limit of STM and the upper limit of LTM were identified (4). By using a constraint condition that the maximum trajectory frequencies exist both within the frequency ranges of USR and outside USR, the residual functions of LTM and STM were determined, and the frequency ranges of LSR and USR identified.

### Method of calculating GT of LTM and STM

Setting LSR and USR as frequency ranges for analysis, Fig. 6 shows a flowchart for calculating two GTs: the frequency gradient of LTM (gradient of tangent of LTM, hereafter abbreviated as GT of LTM), and the frequency gradient of STM (gradient of tangent of STM, hereafter abbreviated as GT of STM).

From the residual function diagram of LTM and STM, the frequency ranges for analysis were identified, and the best approximation curves of LTM and STM are created to calculate their GTs. The best approximation curves are expressed with cubic and quartic functions. In the case of a cubic function, it has one GT, while in the case of a quartic function, it has two IPs, so that two tangent lines and one double tangent are calculated. From these three tangent lines, GT of LTM and GT of STM are calculated.

### Creation of three-dimensional response surface and determination of quartic polynomial expressing characteristics of response surface

Figure 7 shows a three-dimensional response surface and cross sections using the GT of LTM and GT of STM from 225 cases in 137 subjects, a quartic polynomial indicating the response surface, a correlation diagram of SBP-e SBP, and an error analysis diagram.

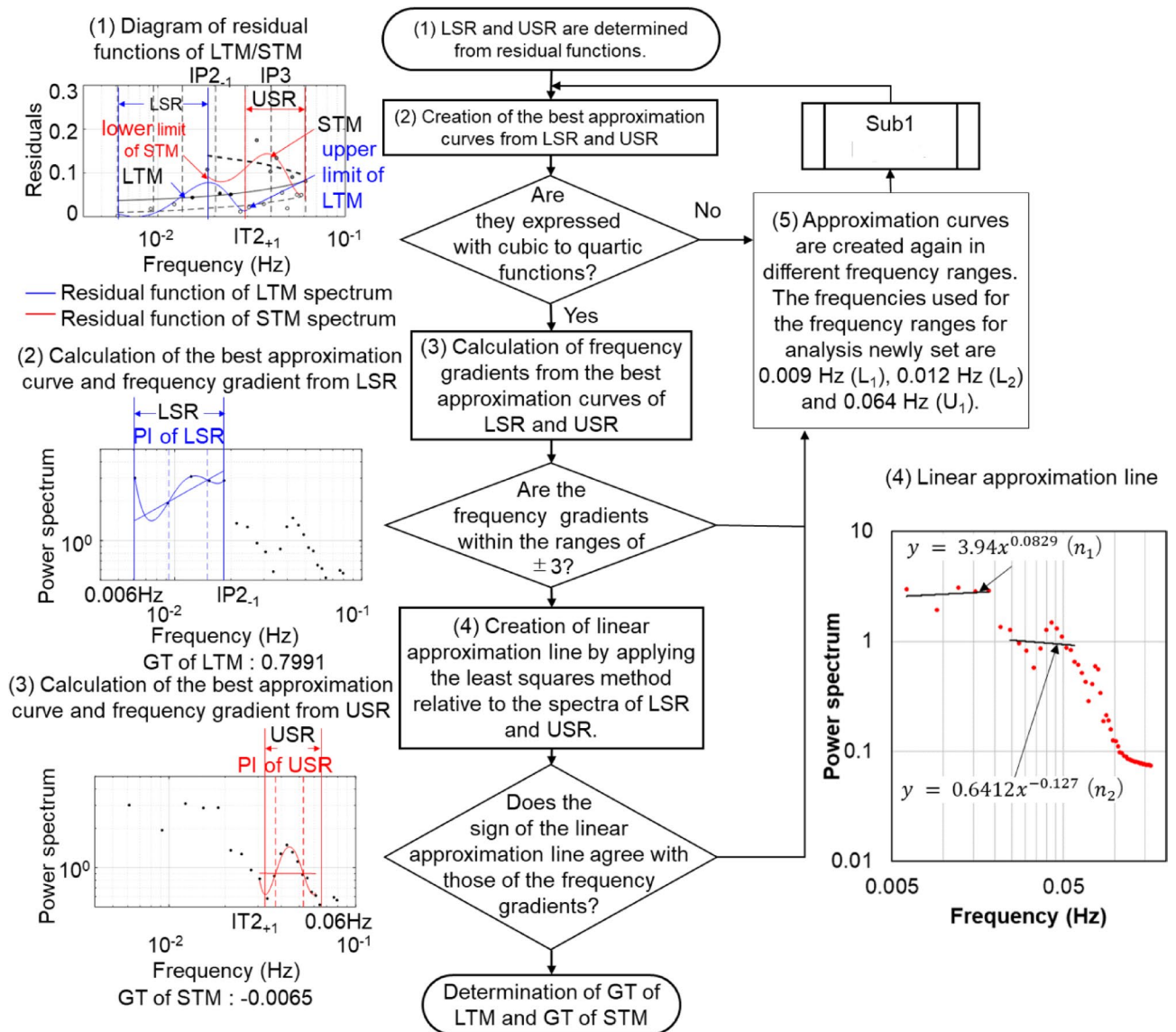
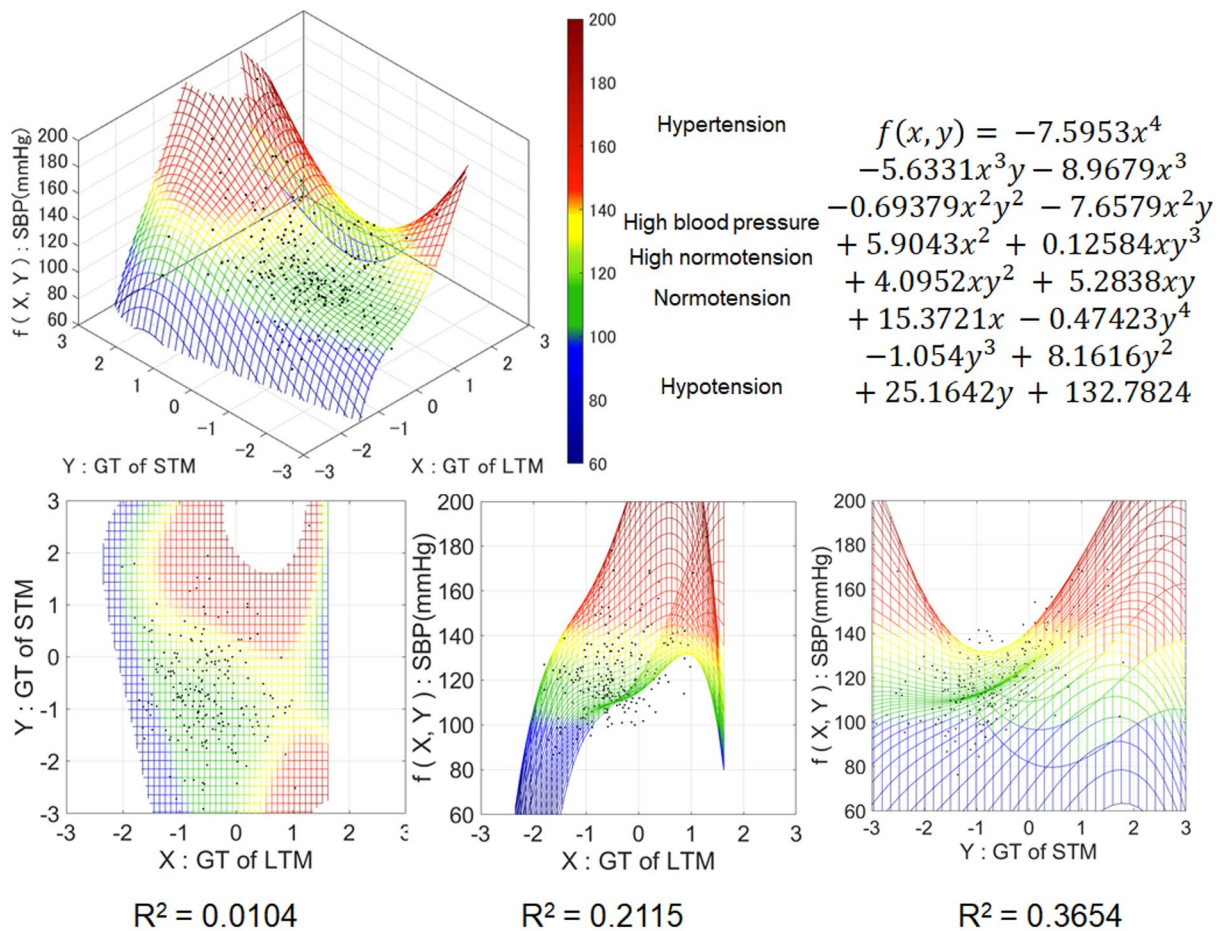


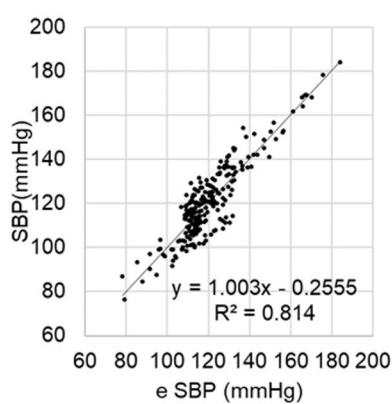
**Fig. 6.** Flowchart for calculating GTs of LTM and STM. In the residual function diagrams of LTM and STM (1), USR and LSR were set, the best approximation curve expressed with a quartic function was created (2)(3), and GTs were calculated via the double tangent. In cases where the function cannot be created, recalculation is conducted by changing the frequency ranges for analysis (5). In a spectrum diagram of a double logarithmic graph, curves having large approximate errors tend to occur on the ends of the low frequency side and the high frequency side. In cases where the three points at the end are linked with a parabola, the errors are small, but when a parabola is drawn with two points, errors occur. If two points are linked with a straight line, errors are few. Accordingly, in the end parts on the low frequency side, frequencies for analysis are extended to the two frequencies of 0.009 Hz ( $L_1$ ) and 0.012 Hz ( $L_2$ ), while in the end parts on the high frequency side, frequencies for analysis are extended to the two frequencies of 0.064 Hz ( $U_1$ ) and 0.08 Hz ( $U_2$ ). The analysis is conducted in the order of subscripts. Incidentally, L is an abbreviation of Lower, which means frequencies on the low frequency side, and U is an abbreviation of Upper, appertaining to frequencies on the high frequency side. Successively, in the frequency ranges of LSR and USR, a linear function is created (4) via the least squares method. The differential coefficient which the linear function has corresponds to GTs  $n_1$  and  $n_2$  expressed in Fig. 4. The agreement of the signs of these GTs with those of LSR and USR obtained from the approximation function was checked

GT of LTM and GT of STM calculated from the IPCM approximation curve are independent variables ( $R^2 = 0.0136$ ), while SBP is a quantity of state simultaneously measured and a criterion variable.

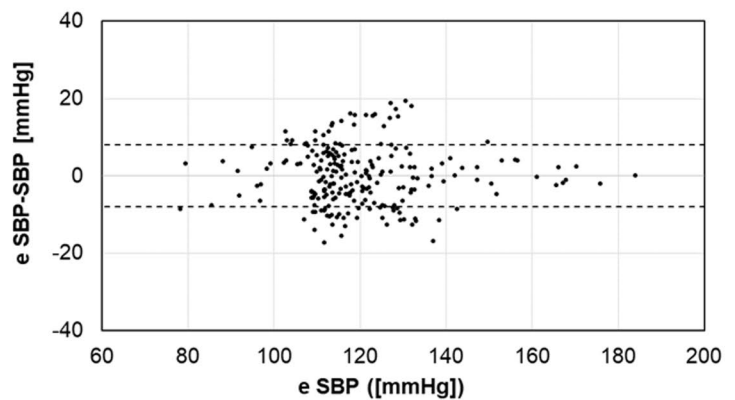
The coefficient of determination of SBP and GT of LTM is  $R^2 = 0.2065$  and that of SBP and GT of STM is  $R^2 = 0.3486$ , which results in weak to medium correlations. We believe that the difference between the two coefficients of determination was the influence of the non-nervous control of LTM and the nervous control of STM. Further, there is a high percentage of aged persons within the subjects of this study. It is known that the dispersion of



(1) Three-dimensional response surface and quartic polynomial



(2) SBP-e SBP correlation diagram



(3) Error analysis diagram

**Fig. 7.** Three-dimensional response surface (SBP, GT of LTM, GT of STM), correlation diagram of SBP-e SBP, error analysis diagram (137 subjects, 225 cases). The three-dimensional response surface is created by curve-fitting using the least squares method. The characteristics of the surface are indicated with a quartic polynomial, and using this quartic polynomial enabled us to estimate SBP. On the three-dimensional response surface (1), the dispersion of blood pressure is large between normotension and high normotension. On the correlation diagram of SBP-e SBP (2) and error analysis diagram (3), the dispersion up to high blood pressure is large. It is known that the heartbeat 1/f fluctuation contributes to the stabilization of blood pressure. Accordingly, this means that there is little 1/f fluctuation in this range. From the correlation diagrams of Mean-SD in Fig. 1 and in Fig. 2, it indicated that the dispersion of heartbeat rhythms was large in the 225 cases. It is assumed that the expanse of the dispersion of SBP between 110 and 140 mmHg was due that the 1/f fluctuation of heartbeat from nervous control was reflected on GTs

heartbeat rhythm of aged persons is smaller, while the dispersion of blood pressure is conversely larger<sup>11</sup>. The dispersion that occurred in the range between 110 and 140 mmHg shown in the correlation diagram of SBP-e SBP and error analysis diagram suggested the involvement of these controls.

Since RAS is a control system<sup>12</sup> with blood pressure as the main control, the cross section of the three-dimensional response surface of SBP-GT of LTM moved upward and to the right. In contrast, the cross section of the three-dimensional response surface of SBP-GT of STM was expressed with a concave function with downward convexity in the hypertensive region, while in the area from hypotension to normotension, it was expressed with a convex function having an upward convex. The high normotensive region became the border of these convex-concave functions, which resulted in a saddle point. Accordingly, the cross section of the three-dimensional response surface of SBP-GT of LTM was expressed with a function having a stationary point in the region of hypotension and normotension. It is conceivable that in the three-dimensional response surface, the saddle point and the stationary point indicate that action and compensation are related to reciprocity, and the regions of hypotension to hypertension are related to trade-off<sup>3</sup>.

The three-dimensional response surface having multiple normal distributions and whose SBP contour map indicated a normal mixture distribution, qualitatively varied relative to the criterion variables as shown in the other two cross sections, thus allowing us to estimate SBP. The three-dimensional response surface was created via curve-fitting using the least squares method, and a quartic polynomial showed the characteristics of the surface.

The coefficient of determination of the correlation diagram of SBP-e SBP became  $R^2 = 0.814$ . The average of the errors created from the data of the 137 subjects/225 cases was 4.1 mmHg, and SD of the errors became 8.3 mmHg.

### Blood pressure Estimation experiment using a quartic polynomial

Figure 8 is an analysis diagram showing the 120 cases of a 67-year old subject. In the correlation diagram of Mean-SD, there were five cases with data existing in the dead zone. For the three of them, their RRI was simply extended, and they were deemed not for rejection (1). The other two are cases of PAC, and the outliers were corrected. The detailed examination results are shown in Supplementary Figure S3. The outliers became the arrow part of the instantaneous heart rate time series data, and an abnormal value test was conducted using the ECG RRI time series data.

Successively, GT of LTM and GT of STM were plotted for the 120 cases on the three-dimensional response surface (2) in Fig. 7, although there was a weak correlation ( $R^2 = 0.2361$ ) downward to the right. Next, the correlation diagram of SBP-e SBP ( $R^2 = 0.8564$ ) and an error analysis diagram are shown. The estimated SBP calculated using the quartic polynomial created from the 225 cases of 137 subjects shown in Fig. 7 was within an estimated precision of  $\pm 3.56$  mmHg. The Mean of the errors was  $-0.5$  mmHg, and SD of the errors became 3.56 mmHg.

These results suggest that the data of the 67-year old subject does not contain the dispersion factors of heart rate variability one sees in the individual differences contained within the data created via the 225 cases (137 subjects). As for the dispersion factor contained in the individual data of one subject, the influence of cardiac contraction and nervous control was larger than that of heart rate variability. As a result, the dimension of the control became low and the minimum of information was applicable, making Mean-SD closer to a normal distribution. Conversely, it is assumed that when the dispersion factors of heart rate variability are contained, the coefficients of determination of GT of LTM and GT of STM on the SBP contour map may decrease.

### Discussions

In Supplementary Fig. S1, the concept, application and correspondence table of this study are shown. The correspondence table is a map related to the abnormal value test from an ECG for 360 s,  $\theta_{i-0}$  time series analysis, the creation of IPCM approximation curves, calculation of GTs using residuals, and creation of a three-dimensional response surface via GTs and SBP. By plotting the time series waveforms used for a short-time heart rate variability analysis alongside the  $\theta_{i-0}$  time series waveforms, the existence of the control mechanism working in limited periods for regulating each function of the organs was demonstrated, along with the control mechanism working in the entire period for regulating the relationship between the organs in the whole body, and their reciprocal and trade-off relationship was also indicated.

By considering the time series analysis together with the results of the frequency analysis, the existence of GTs producing changes in state became apparent. Further, the relation of GTs smoothing the changes in state was also shown. The three-dimensional response surface composed of GTs of LTM and STM, and their dependent variable SBP visualized the degree of stability of the control results via IPCM.

The GTs of LTM and STM are basically energy variation information on the action and compensation of the arterial pressure control systems, which suggests that the correlation of the two action forces might be obtained from the frequency information. It is high-order data, the GTs of the energy variation information alone having ten possible combinations. For the combinations of the energy variation information and frequency information, if they have characteristics, symmetry, similarity and compositionality as a manifold, the number of dimensions will further increase by fractionating the frequency information. It was also suggested that data generation using AI might enable us to grasp the working of the factors varying the timing of the change in state and homeostasis of the state, which may bring forth new biological information.

When simultaneously recording ECG information with the two-dimensional delay coordinate system Lorenz plot diagram for 360 s, visualizing the dispersion state of heart rate variability, and the correlation diagram of Mean-SD obtained from the three-dimensional delay coordinate attractor diagram for 360 s utilized for analyzing noise and errors, the resulting data may be used as an auxiliary diagnostic tool for rhythm analysis. It

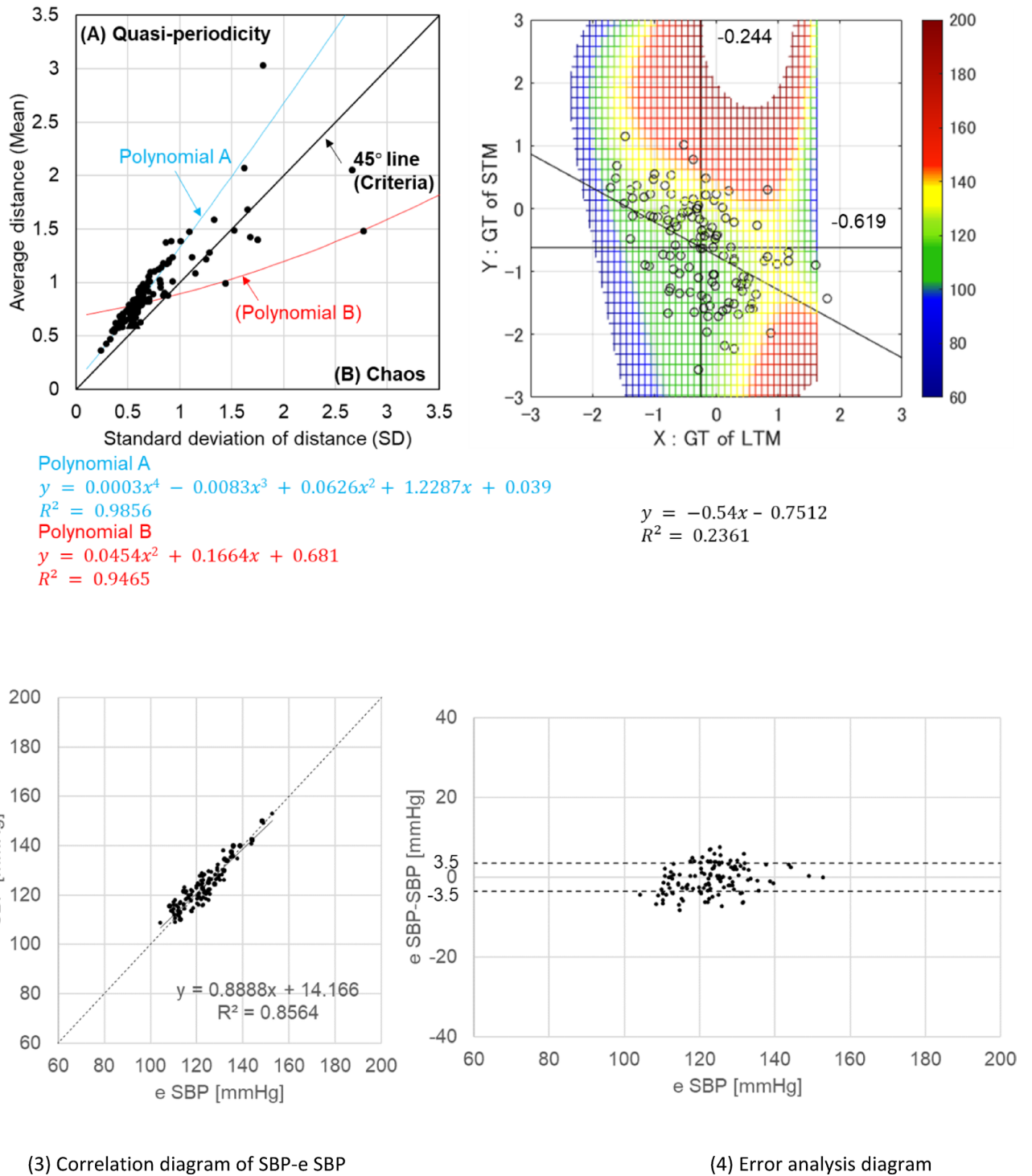


**Fig. 8.** Examination of estimation precision of SBP (120 cases using a 67-year old subject) via a correlation diagram of Mean-SD, SBP contour map (GT of LTM, GT of STM), correlation diagram of SBP-e SBP, error analysis diagram. In the 120 cases, the variation of heartbeat rhythms is small, as can be seen from the dispersion state of the clusters on the correlation diagram of Mean-SD (1). The clusters are in the vicinity of Polynomial A and the 45° line. The barycenter of the clusters of the 120 cases on the SBP contour map (2) created from the three-dimensional response surface in Fig. 7 became (GT of LTM, GT of STM) = (-0.244, -0.619) and was in the vicinity of SBP = 120 mmHg. The expanse of 110 to 140 mmHg on the correlation diagram of SBP-e SBP (3) and the error analysis diagram (4) became smaller compared with that of Fig. 7. Since it does not contain the dispersion factors of heart rate variability due to the data coming from just one person, it can be assumed that the effects of cardiac contraction and nervous control may have been larger than that of heart rate variability

is conceivable that the method of extracting phase information allows us to grasp the influences of reciprocal and modification factors added to biological information more comprehensively. By changing analysis procedures and measurement time, a paired analysis can be conducted.

Further, the quartic polynomials obtained in this study could be used for SBP estimation. In addition, 118 cases of normal heart rate and two cases of arrhythmia could be also extracted. By examining them together with the ECG information, the cases of PAC and the ones in which the RRI was simply extended could be also judged. The examination background using a Lorenz plot, attractors, best approximation curves and GTs are shown in Supplementary Fig. S3. In three cases, instantaneous heart rate time series data showed abnormal values that would normally be rejected. By using modified attractors, new instantaneous heart rate time series data was created, and the Mean and SD could be recalculated. The results then replotted on the correlation diagram of Mean-SD to determine whether the corrected results were good or bad.

The Guyton extended model composed of IPCM and multiple control mechanisms has an energy variation amount indicating probability distribution as an index. The arterial pressure transient response via the non-neural intermediate pressure control mechanism can capture chaotic variations from analysis for 360 s (with 30 s segments); these chaotic variations are regulated with an energy variation index (derivative action index: GT). We have devised a method of classifying power spectra dispersed to calculate energy variation indexes representing action and compensation, by using residual functions. The results of the estimation of SBP experiment showed that the combination of Newtonian mechanics defined with displacement, velocity and acceleration with the chaos time series analysis, conducting analysis with dispersion including probability distribution, suggested that a mathematical analysis might explain the physiological action and compensation.

For the parameters used for analysis, action and compensation are represented with frequency gradients on condition that the energy variation index is constant through the use of the principle of least action. It was assumed that for hypotensives, a pressor action was present, while for hypertensives, it was a depressor action, and that reciprocal compensation relative to each action functioned. Since there are two inflection points in the range between hypotension and hypertension, a response surface can be expressed with a quartic expression. It is believed that the possibility of bias regarding the aforesaid flow of algorithm is low.

In the present study, the measurement of the 137 subjects is one of the limitations. In the future, there may be a little variation in the coefficients of the quartic expressions of the response surfaces following an increase in the number of subjects for measurement. Also, since the subjects of this study are people who can live a normal life (or outpatients), it is not entirely clear if this study is applicable to patients in hospital or those with critical diseases. However, since this method has high affinity with generative AI, in the future, we consider that it will be useful for developing applications to telemedicine and home nursing.

To evaluate the constant variations in a person's blood pressure, this paper estimates SBP by using electrocardiogram data taken for six minutes (360 s). As a result, the mean of the two values before and after the measurement of electrocardiogram and correlation were obtained. Although a measurement of six minutes was chosen, it is conceivable that further continuation of the measurement enables us to estimate blood pressure value at each point in time, which has significant clinical value. In the future, it is expected that the measurement time frame can be shortened.

## Data availability

The datasets used and/or analysed during the current study available from the corresponding author on reasonable request.

Received: 20 March 2025; Accepted: 10 October 2025

Published online: 17 November 2025

## References

- Hall, J. E. *Guyton and Hall Textbook of Medical Physiology 13th edition*, 215–246 (Elsevier, 2016).
- Cowley, A. W. Jr., Liard, J. F. & Guyton, A. C. Role of the baroreceptor reflex in daily control of arterial blood pressure and other variables in dogs. *Circ. Res.* **32**, 564–576. <https://doi.org/10.1161/01.RES.32.5.564> (1973).
- Hatakeyama, T. & Kaneko, K. Robustness and plasticity in biological rhythms. *Seibutsu Butsuri*. **57**, 186–190. <https://doi.org/10.2142/biophys.57.186> (2017).
- Maeda, Y., Sekine, M., Tamura, T. & Mizutani, K. Effect of pulse arrival time variability on the difference between heart rate variability and pulse rate variability. *Trans. Japanese Soc. Med. Biol. Eng.* **54**, 261–266. <https://doi.org/10.11239/jsmb.54.261> (2016).
- Sakata, A. & Kaneko, K. Evolutionary dimensionality reduction supporting robustness and plasticity in biological systems. *Brain Neural Networks*. **31**, 149–159. <https://doi.org/10.3902/jnns.31.149> (2024).
- Nobuhiro, Y. et al. Kaosu Kaiseki Wo Mochiita Junkandoutaishihyou no Kentou (In Japanese). *Japan Soc. Des. Eng. Chugoku Branch. Lecture Papers*, 46–50 (2024).
- Tsuda, I. & Matsumoto, K. Noise-induced order. *Butsuri* **40**, 203–207. <https://doi.org/10.11316/butsuri1946.40.203> (1985).
- Kamo, T. et al. Spectral analysis of blood pressure and blood flow velocity in the middle cerebral artery using the maximum entropy method (MEM). *Neurosonology* **6**, 2–8. <https://doi.org/10.2301/neurosonology.6.2> (1993).
- Akselrod, S. et al. Hemodynamic regulation: investigation by spectral analysis. *Am. J. Physiol. Heart Circ. Physiol.* **249** <https://doi.org/10.1152/ajpheart.1985.249.4.H867> (1985). H867–H875.
- Fujita, E. et al. Development of the measurement method of the prediction of sleep by finger plethysmogram data. *Japanese J. Ergon.* **41**, 203–212. <https://doi.org/10.5100/jje.41.203> (2005).
- Castiglioni, P., Frattola, A., Parati, G. & Rienzo, M. D. 1/f-Modelling of blood pressure and heart rate spectra: Relations to ageing, *14th Annual International Conference of the IEEE Engineering in Medicine and Biology Society*, 465–466, 465–466, (1992). <https://doi.org/10.1109/IEMBS.1992.5761062> (1992).
- Noguchi, K., Fukamizu, A. & Yamagata, K. Jinzou to RAS (In Japanese), Yamaguchi Endocrine Research Foundation, (2014). <http://www.yamaguchi-endocrine.org/pdf/noguchi.pdf>

## Acknowledgements

We would like to thank Dr. Shigehiko Kaneko, Emeritus Professor of University of Tokyo, Dr. Masashi Kawamoto, Emeritus Professor of Hiroshima University and Dr. Yuji Tsuchida, Professor of Oita University. For English translation, we received support from Mr. Brian Long, Mr. Takaharu Kobayakawa and Mr. Masashi Iwatani.

## Author contributions

E.F. devised hypotheses and analyzed experimental data, Y.O. managed the study, R.U. was in charge of experiments and data analysis with algebraic equations, Y.N. was in charge of data analysis of chaos time series analysis, S.M. was in charge of development of application for mathematic analysis, S.K. was in charge of frequency analysis. M.Y. made discussions of the hypotheses and interpretation of the experimental data, K.M., S.I., K.T., T.K. and H.T. conducted experiments, and K.M. and T.K. revised the discussions and articles for improving scientific values.

## Declarations

### Competing interests

The authors declare no competing interests.

### Additional information

**Supplementary Information** The online version contains supplementary material available at <https://doi.org/10.1038/s41598-025-24106-4>.

**Correspondence** and requests for materials should be addressed to E.F.

**Reprints and permissions information** is available at [www.nature.com/reprints](http://www.nature.com/reprints).

**Publisher's note** Springer Nature remains neutral with regard to jurisdictional claims in published maps and institutional affiliations.

**Open Access** This article is licensed under a Creative Commons Attribution-NonCommercial-NoDerivatives 4.0 International License, which permits any non-commercial use, sharing, distribution and reproduction in any medium or format, as long as you give appropriate credit to the original author(s) and the source, provide a link to the Creative Commons licence, and indicate if you modified the licensed material. You do not have permission under this licence to share adapted material derived from this article or parts of it. The images or other third party material in this article are included in the article's Creative Commons licence, unless indicated otherwise in a credit line to the material. If material is not included in the article's Creative Commons licence and your intended use is not permitted by statutory regulation or exceeds the permitted use, you will need to obtain permission directly from the copyright holder. To view a copy of this licence, visit <http://creativecommons.org/licenses/by-nc-nd/4.0/>.

© The Author(s) 2025, corrected publication 2026